5-2021

Electrodeposition of Hydrogen Molybdenum Tungsten Bronze Films and Electrochemical Reduction of Carbon Dioxide.

Mohammad Bajunaid
East Tennessee State University

Electrodeposition of Hydrogen Molybdenum Tungsten Bronze Films and Electrochemical Reduction of Carbon Dioxide CO_2

A thesis

presented to

the faculty of the Department of Chemistry

East Tennessee State University

In partial fulfillment

of the requirements for the degree

Master of Science in Chemistry

by

Mohammad Saeed Bajunaid

May 2021

Dr. Dane W. Scott

Dr. Greg Bishop

Dr. Catherine McCusker

Keywords: electrodeposition, reduction of carbon dioxide, oxalic acid, ion chromatography

ABSTRACT

Electrodeposition of Hydrogen Molybdenum Tungsten Bronze Films and Electrochemical Reduction of Carbon Dioxide CO_2

by

Mohammad Bajunaid

The foremost aim for performing this study was to focus on the electrodeposition of mixed hydrogen molybdenum tungsten bronze films, which have potential for e^- transfer interactions carrying out reduction of carbon dioxide. A yellow peroxymolybdic tungstate solution was prepared and used for the electrodeposition of hydrogen molybdenum tungsten bronze films on conductive carbon paper. Electrodeposition was carried out at -2.0 V from 20 - 120 minutes to determine the effect of deposition time on film thickness and CO_2 reduction. These films were characterized by X-ray photoelectron spectroscopy. The deposited films served as a working electrode for CO_2 electrochemical reduction utilizing 0.8 M $NaHCO_3$ as the electrolyte. Carbon dioxide gas was bubbled into the cathode solution for an hour while bulk electrolysis was carried out at different applied potentials. Products were identified and evaluated using ion chromatography.

DEDICATION

This project is dedicated to my family: my parents, and my friends who have supported me along my journey.

ACKNOWLEDGEMENTS

I would like to thank Dr. Dane Scott for being a great advisor. I also would like to thank my thesis committee members, Dr. Greg Bishop and Dr. Catherine McCusker, for their comments in completing the thesis. X-ray photoelectron spectroscopy data was provided by Dr. Nicholas Materer, Chair of Chemistry at Oklahoma State University. Also, I would like to thank King Saud bin Abdulaziz University for Health and Sciences for giving me a full scholarship to attend ETSU. I also thank the ETSU Office of Research and Sponsored Programs Administration for funding this work.

TABLE OF CONTENTS

LIST OF TABLES

LIST OF FIGURES

LIST OF ABBREVIATIONS

CV	Cyclic voltammetry
CVD	Chemical vapor deposition
FDH	Formate dehydrogenase
FE	Faradaic efficiency
GCP	Global carbon project
GHGs	Greenhouse gases
IR	Infrared
NHE	Normal hydrogen electrode
NP	Nanoporous
SCE	Saturated calomel electrode
SHE	Standard hydrogen electrode
RHE	Reversible hydrogen electrode
XRD	X-ray diffraction
XPS	X-ray photoelectron spectroscopy

CHAPTER 1. INTRODUCTION

Carbon Dioxide

Carbon dioxide (CO_2) is a major by-product that is formed upon combusting fossil fuels. Combusting one ton of fossil fuels results in over 3.5 tons of CO_2.[1] CO_2 is a greenhouse gas that is found to have a close correlation to ocean acidification and global warming.[2] That is because this gas absorbs infrared radiation. As more greenhouse gases (GHGs) are in the air, less heat is released from the earth.[3] The CO_2 concentration in the air has reached historical levels and has been rising over the last few years.[4] The current global average level of atmospheric carbon exceeds 400 ppm, as shown in Figure 1.[5]

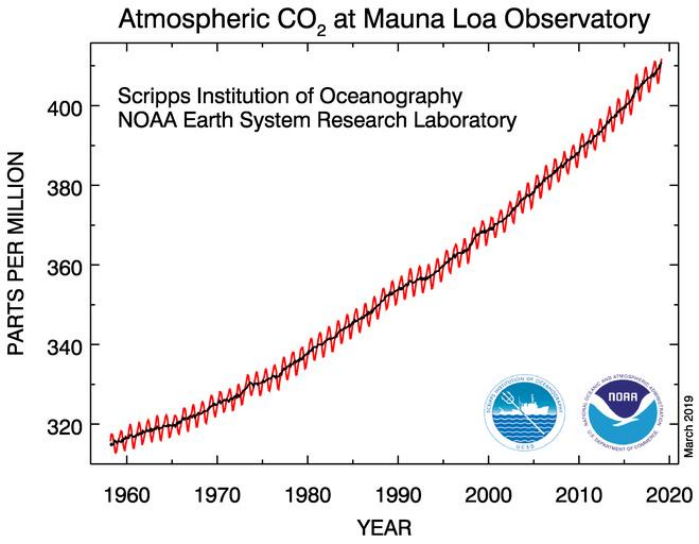

Figure 1. Atmospheric CO_2 levels and year as measured by the Earth System Research Laboratory. Reprinted by permission from NOAA/ESRL Global Monitoring Division Lab.[5]

The amount of atmospheric CO_2 in ppm and year are presented in Figure 1 obtained from the National Oceanic and Atmospheric Administration's Earth System Research Laboratory website.[5] Research has been focused on CO_2 reduction to recycle carbon dioxide and possibly convert CO_2 to feedstocks for energy production.[6] Two examples of useful products from

reduced CO_2 are formate and methanol. These reduction products are of interest as they may be used in fuel cells generating power in the form of current.[7,8] An example is a formate fuel cell operating at 60 °C that produces a power density of 591 mW/cm^2.[9] To realize using CO_2 as a feedstock for fuel cells, reduction of CO_2 must be selective and efficient. Electrochemical conversion is one way to reduce CO_2.

Electrochemical CO_2 Reduction to Formate and Methanol

Electrochemical reduction of CO_2 is capable of generating useful hydrocarbons.[6] Reduction products are hydrocarbons including CH_3OH (methanol), CH_4 (methane), CO (carbon monoxide), $HCOO^-$ (formate) and even oxalate.[10] The reduction steps resulting in formate and methanol, due to being products of interest, are briefly reviewed. Table 1 shows the electrochemical reactions at the cathode, anode, and overall reaction reducing CO_2 to methanol.

Table 1. Electrochemical reaction for carbon dioxide (CO_2) conversion to methanol CH_3OH under standard condition.[11]

	Electrochemical reaction	*E* (V)	
Cathode	$CO_2 + 6H^+ + 6e^- \rightleftarrows CH_3OH + H_2O$	-0.22 vs. SCE	(1)
Anode	$3\ H_2O \rightleftarrows 1.5\ O_2 + 6H^+ + 6e^-$	0.99 vs. SCE	(2)
Overall	$CO_2 + 2\ H_2O \rightleftarrows CH_3OH + 1.5O_2$	1.21	(3)

Figure 2 shows the two most probable reaction pathways for the electrochemical reduction of CO_2 that result in formate and methanol. The 1st mechanism (a) proceeds through generating CO, and the 2nd mechanism (b) through the formate ($HCOO^-$) intermediate.

(a) $CO_2 + e^- + H^+$ (at the cathode surface) $\rightarrow HOCO^-$ $E° = -0.125$ V $HOCO^- + e^- + H^+ \rightarrow H_2O + CO$ $E° = -0.106$ V $CO + e^- + H^+ \rightarrow HCO$ $E° = -0.125$ V $HCO + e^- + H^+ \rightarrow CH_2O$ $E° = -0.024$ V $HCHO + 2e^- + 2H^+ \rightarrow CH_3OH$ $E° = +0.16$ V	
Overall: $CO_2 + 6H^+ + 6e^- \rightarrow CH_3OH + H_2O$ $E° = -0.22$ V	(4)
(b) $CO_2 + e^- + H^+ \rightarrow HCOO^-$ $E° = -0.210$ V $HCOO^- + e^- + H^+ \rightarrow HCOOH$ $E° = -0.150$ V $HCOOH + e^- + H^+ \rightarrow HCO + H_2O$ $E° = -0.210$ V $HCO + e^- + H^+ \rightarrow CH_2O$ $E° = -0.06$ V $HCHO + 2e^- + 2H^+ \rightarrow CH_3OH$ $E° = +0.41$ V	
Overall: $CO_2 + 6H^+ + 6e^- \rightarrow CH_3OH + H_2O$ $E° = -0.22$ V	(5)

Figure 2. Most probable reaction pathways in the CO_2 electrochemical reduction to CH_3OH, via intermediates of (a) CO and (b) HCOOH.[11,12,13]

Another possible reduction product is oxalate.

Electrochemical CO_2 Reduction to Oxalate

Conversion of CO_2 to oxalate is important due to the results obtained in this work. There are numerous reports on CO_2 reduction to oxalates using low-valent d and f block metals.[14,15] The standard reduction potential for CO_2 to oxalate is -0.590 V vs. the SHE.[16] Just this year (2020), a stainless-steel electrode in acetonitrile with CO_2 at 2 atm using a current density of 15 mA/cm^2 resulted in production of oxalate with an average Faradaic efficiency of 78%.[15] A stainless-steel electrode is beneficial over other metal electrodes because it does not corrode and promote electroreduction of CO_2.[17,18] In another study, a binuclear Cu (I) complex consisting of $[Cu_2(m\text{-xpt})_2]$ $(PF_6)_2$ was found to reduce CO_2, resulting in a bridged oxalate ion between two

Cu^{2+} ions.[14] The bound oxalate ions are removed as oxalic acid upon reaction with mineral acids. The copper (I) complex can be regenerated using ascorbate as a moderate reducing agent.[14]

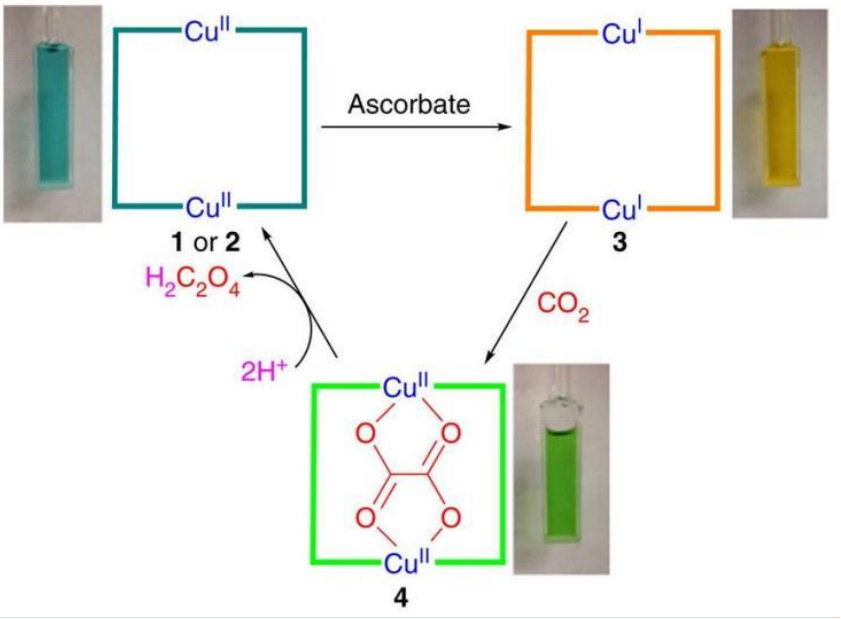

Figure 3. he preliminary copper (II) complexes (1= $[Cu_2(m\text{-xpt})_2(NO_3)_2]$ $(PF_6)_2$ and 2= $[Cu_2(m\text{-xpt})_2Cl_2]$ $(PF_6)_2$) are reduced in the existence of sod. ascorbate to Cu(I) complex (3= $[Cu_2(m\text{-xpt})_2]$ $(PF_6)_2$). The CO_2 reacts then with the later complex to yield oxalate-bridged complex (4= $[Cu_2(m\text{-xpt})_2(\mu\text{-}C_2O_4)]$ $(PF_6)_2$). The oxalate is converted to oxalic acid upon reacting acids with complex 4, renewing the preliminary 'empty' complexes again.[14] Reprinted by permission from [the Licensor]: [Springer] [Nature Communications] [(Reduction of carbon dioxide to oxalate by a binuclear copper complex, Pokharel, UR., Fronczek, FR. & Maverick, AW.), [COPYRIGHT] (2014), (doi.org/10.1038/ncomms6883.[Nat. Comm]).[14]

To produce methanol, formate, and oxalate selectively and efficiently, metal modified and metal supported carbon electrodes have been used.

Metal Electrodes for CO_2 Reduction

Copper was first used in 1985 to reduce CO_2.[19] Other metals have been used for CO_2 reduction and are classified into four groups based on the main product they produce. Pb, Hg, Ti, In, Sn, Cd and Bi produce formate, Au, Ag, Zn, Pd and Ga produce carbon monoxide, Ni, Fe, Pt,

and Ga reduce a small amount of CO_2 and produce H_2 from water. These differences in selectivity and product formation are considered to be due to the binding energy of key intermediates in reduction of CO_2 which occupy catalytic active sites.[20] Pure copper stands out due to being able to reduce CO_2 to multiple products requiring two or more electrons for reduction of CO_2. These include methane, ethane, ethanol, propanol, formate, carbon monoxide.[20] Metal electrodes at a pH of 6.8 using 0.1 M $KHCO_3$ as an electrolyte are known to result in Faradaic efficiencies near 100% when summing liquid and gaseous products.[21] Producing formate requires an overpotential of 1.1 V vs. the RHE. Copper produces hydrocarbons and oxygenated hydrocarbons at a potential of 1.0 V vs. RHE and at an overpotential of 0.9 V, before formate is produced, CO_2R products are converted to carbon monoxide. At an overpotential of 1.2 V methane is a main product.[20] One goal is selective reduction meaning one product is favored over another. As an example, Ru, Cu-Cd modified Ru, and Cu-Cd modified Ru and Iridium oxides have been used having Faradaic efficiencies ranging from 15.3 to 38.2% at applied potential of -0.8 V vs. SCE in 0.5 M $NaHCO_3$ electrolyte solution.[11] Methanol was found to be the main product.[11] Another strategy for selective electrochemical CO_2 reduction is using metals and metal alloys supported on carbon.

Recent Carbon Supported Metal and Metal Alloys for CO_2 Electrochemical Reduction

Carbon supports have the ability to enhance metal dispersion improving selectivity and/or activity of the supported electrocatalyst.[22] A Pb-Sn alloy on a carbon support is such an example used in the reduction of CO_2. Both CV and XPS showed that these supported metals formed oxides. The FE employing the Pb-Sn alloy for the formate production was 79.8%, at -0.6 V compared to the silver chloride reference electrode, which is higher than Pb or Sn alone by 16%.[23] Pt and Pd were employed as an alloy for CO_2 electrochemical reduction. A Pd/Pt catalyst

on a C-film support was used for CO_2 electrochemical reduction to formate at low overpotentials. The supported Pd-Pt nanoparticles have the capability for reducing CO_2 to formate starting at –0.05 V.[24] Furthermore, a 70 % Pd: Pt 30% alloy resulted in an FE of 88% for formate after 1 hour of electrolysis at -0.4 V. Nonetheless, reduction was restricted due to formation of CO at the surface of the catalyst.[24] Carbon supported Pd nanoparticles are an example in which the CO_2 reduction Faradaic efficiency reached 97%. However, the Faradaic efficiency dropped swiftly, after one hour, due to catalytic poisoning. Embedded Pd in carbon ink on titanium foil achieved CO_2 electrochemical reduction. In 0.5 M $NaHCO_3$ saturated with CO_2, the Faradaic efficiency decreased at -0.35 V by 80% after 3 hours.[25] Carbon electrocatalysts doped with N atoms, Co, Ni, and Fe achieved CO_2 reduction to CO, requiring an overpotential of 0.560 V with a Faradaic efficacy of 93%.[26] The Faradaic efficacy dropped over 2 hours and maintained an efficiency of 63% for the remaining 12 hours.[26] In many of these examples, the reduction of CO_2 requires a high overpotential, have low selectivity and activity decreases over time.[27] One reason for a decrease in Faradaic efficiency is carbon monoxide poisoning.

Carbon Monoxide Poisoning

Carbon monoxide (CO) is a typical byproduct which forms at -0.11 V vs. the RHE.[28] Using an overpotential to generate hydrocarbons from CO_2, CO is almost always generated to some degree. Once CO is formed, all metals have a positive adsorption energy for CO, except for copper. This is due to the positive binding energy copper has for CO, + 0.1 eV.[20] Carbon monoxide (CO), an intermediate, deactivates the catalyst, referred to as poisoning, by adsorbing which blocks active sites of the catalyst.[29] Poisoning is characterized by the steady degradation of the catalytic ability toward product formation observed as a decrease in measurable current. For example, in the case of Pd supported on carbon, after 3 hours electrochemical reduction of

CO_2 to formate is inhibited by generation of CO.[25] Due to such issues as CO poisoning of electrocatalysts for CO_2 reduction, selectivity and efficiency new and different catalysts are desired.

Selection of Hydrogen Bronzes for Electrochemical Reduction of CO_2

Hydrogen bronze is the name given to a metal oxide with hydrogen ion. An example is hydrogen molybdenum bronze, H_xMoO_3, in which x is between 0.46 and 1.63.[30-32] Hydrogen molybdenum bronze is blue in color.[33] Other examples of metal oxides that form hydrogen bronzes include tungsten and vanadium oxide.[34] Many methods are used for preparing hydrogen bronze films include sol-gel approaches, ammonium-heptamolybdate thermal decomposition, or metal vapor deposition followed by oxidation and addition of hydrogen using zinc and HCl.[34-38]

In solution, hydrogen molybdenum bronze is easily generated by adding zinc to a solution of MoO_3 solid in an aqueous solution of HCl which generates hydrogen ion. The generated hydrogen in contact with the WO_3 surface undergoes dissociative chemisorption and diffuses into the metal oxide matrix turning yellow MoO_3 blue and results in molybdenum having a mix of 5^+ and 6^+ oxidation states.[39] During the reaction, the color changes from pale green for pure WO_3 to blue for treated WO_3. The W atoms are reduced by 0.5 M HCl to W^{5+} or W^{6+} resulting in H_xWO_3 following injection of H^+ ions into the oxide matrix.[33] The coating effective surface electronic resistivity (ρ_S) has been measured, and the results demonstrated a decrease in the ρs upon injection of H^+ ions. The primary implication is that the crystal structure of the doped H^+ ions from H_xWO_3 improved electrical conductivity. Thus, this evidence reveals that H_xWO_3 has a strong metallic character, which is attributed to the intercalation of H^+ ions into WO_3 lattice. The result is an increase in donor energy and charge carries.[33]

Formation of hydrogen bronzes also result when using water and hydrogen gas. Oxygen vacancies exist represented by the 3-x subscript in the blue hydrogen molybdenum bronze product shown in equation (6).[40]

$$\tfrac{1}{2}\ yH_2 + Mo^{VI}O_3 \rightarrow H_yMo^{V/VI}O_3 \rightarrow \mathbf{H_yMo^{V/VI}O_{3-x}} + xH_2O \quad (6)$$

The oxygen vacancies in a hydrogen bronze when optimized contribute to increasing light absorption, electron-hole recombination, increased conductivity, and most importantly, improved electrocatalysis.[41-46] Another study characterized $Mo_xW_{1-x}O_3$ films. They found several oxides present as W_xO_{3x-1}, such as W_3O_8, W_4O_{11}, W_8O_{23}.[47] This makes it difficult to determine the stoichiometry of bronze formed, and the actual molecular composition since characterizing the as-deposited amorphous are difficult to determine using both electrochemical quartz crystal microbalance (EQCM) methods and conventional surface analytical techniques. Hydrogen bronzes may also be prepared by electrodeposition from metal peroxy acid solutions. Electrodeposition from a mixture of peroxymolybdic and peroxytungstic acids, described below, was successful and XPS confirmed the presence of both molybdenum and tungsten.[47]

Peroxymolybdic and Peroxytungstic Acid Solutions

Hydrogen bronze films may be prepared by electrochemical deposition on metal substrates from peroxymetal solutions.[48] Two common methods are employed to prepare the solution from which hydrogen bronze films may be prepared by electrodeposition: sodium molybdate dissolved with the addition of hydrogen peroxide H_2O_2 and molybdenum metal dissolved directly with H_2O_2. The prepared solution also serves as the electrolyte for electrodeposition.[49] Equation (7) shows the reaction forming peroxymolybdate.

$$[MoO_4]^{2-} + 2\ H_2O_2 \rightleftharpoons [MoO_2(O_2)_2]^{2-} + 2\ H_2O \quad (7)$$

After adding acid shown in Equation (8), the solution turns yellow.

$$H^+ + [MoO_2(O_2)_2]^{2-} \rightleftharpoons [HMoO_2(O_2)_2]^{2-} \quad (8)$$

The yellow color fades due to decreasing H_2O_2 over time.[49] It was established that adding additional H_2O_2 caused the yellow color to return.[49] In the same way, peroxytungstate acid may be prepared. Sodium tungsten dissolution with the addition of hydrogen peroxide H_2O_2 is shown in Equations (9) and (10).[50]

$$[WO_4]^{2-} + 2\ H_2O_2 \rightleftharpoons [WO_2(O_2)_2]^{2-} + 2\ H_2O \quad (9)$$

$$H^+ + [WO_2(O_2)_2]^{2-} \rightleftharpoons [HWO_2(O_2)_2]^{2-} \quad (10)$$

In this work, a mixed peroxy molybdate tungstic acid solution was prepared to electrodeposit a hydrogen molybdenum tungsten bronze film.

Use of Hydrogen Bronze for CO_2 Reduction

Hydrogen bronzes themselves are known to have high surface area (30 m^2/g^{-1}) making them capable of serving as a catalyst and/or catalytic support.[51] A recent thesis has shown that nickel coated MoO_3 and WO_3 as a hydrogen bronze in the presence of hydrogen gas is capable of photocatalytic reduction of CO_2.[40] The amount of CO_2 converted to methane increased with temperature and when illuminated using a 300 W Xenon light source compared to dark conditions. At 200 °C, CO_2 was converted at a rate of 20 µmole/g/hr in the dark compared to 80 µmole/g/hr when illuminated using 5% by mass loading of nickel on the hydrogen bronze.[40] The rate of CH_4 formation was shown to be stable over 12 hours. In this same study, WO_3 without nickel illuminated for one hour using a 1:1 ratio of CO_2 and H_2 at 2 atm was shown to produce CO at a rate of 5 µmole/g/hr.[40] This result leads to the idea and motivation of using hydrogen bronzes as a potential electrocatalyst supported on carbon for stable and selective electrochemical reduction of CO_2.

Motivation for Current Research Work

Dr. Scott's research using hydrogen molybdenum bronze films supported on carbon paper was shown to reduce CO_2 to formate electrochemically.[52] However, due to only obtaining a Faradaic efficiency of 8% for formate at an applied potential of -0.4 V vs. the silver chloride reference electrode, these results were not ideal, and no CO gas was detected in the headspace.[52] Bimetal oxides compared to single metal oxides have been shown to increase reaction rates due to having a greater number of acidic or basic sites and/or increased surface area.[53-57] An electrochemical example of this strategy is a study which used the combination of CuO and ZnO as a gas diffusion electrode for reduction of CO_2. Methanol was formed with an efficiency of 17% and a selectivity of 88% at -1.32 V. Use of CuO and ZnO resulted in reduced selectivity for methanol.[58] As there are three metal oxides that result in hydrogen bronzes, a mixed molybdenum tungsten hydrogen bronze film was chosen to use first for electrochemical conversion of CO_2. The mixed hydrogen bronze films were prepared on carbon paper by electrodeposition and characterized by voltammetry.

CHAPTER 2. EXPERIMENTAL METHODS

Materials and Chemicals

Both N_2 and CO_2 gases were purchased from Airgas. The Na_2SO_4 (Salt bridge/0.2 M), conductive carbon-paper with a resistivity of 80 mΩ·cm, NaOH, $NaHCO_3$, sodium molybdate dihydrate, and sodium tungstate were purchased from VWR. A solution of Na_2CO_3 (3.6 mM) was utilized as the mobile phase for performing ion chromatography to quantify the product.

Equipment

Two beakers serving as an anode and cathode compartment were connected with a fritted salt bridge (0.2 M Na_2SO_4). The CHI 604 E using software version 15 was used to carry out electrodeposition, cyclic voltammetry studies, and electrochemical reduction. All stated potentials are in reference to the silver chloride reference electrode. Product was quantified by using a Metrohm 930 Ion Chromatogram.

Electrodeposition of Tungsten Molybdenum Hydrogen Bronze Films

Hydrogen molybdenum tungstate bronze films were prepared on carbon paper by electrodeposition using by modifying reported procedures.[47,52,59-61] The method involves reacting molybdenum powder or metal with H_2O_2 creating peroxymolybdic acid, which acts as the electrolyte for electrodeposition. Approximately 2.42 g of sodium molybdate dihydrate was dissolved in 30 mL of 10% sodium tungstate and 22 mL of 3% H_2O_2 was added resulting in a yellow solution of peroxymolybdic tungstate acid, which was stirred overnight. About 22 mL of 3% H_2O_2 was then added, followed by conc. H_2SO_4 dropwise for adjusting the pH of the solution to 2 measured using a calibrated Vernier® pH electrode. The yellow peroxymolybdic tungstate solution was used for the deposition of molybdenum and tungsten bronzes films. The

experimental setup is shown below in Figure 4. A 3-electrode scheme was utilized in which the Ag/AgCl electrode was employed as a reference, an inexpensive wire mesh platinized titanium anode was used as the counter electrode and carbon paper (1 in x 3 in) was the working electrode for depositing the hydrogen molybdenum tungsten bronze films. While the active area of the counter electrode is not known or was measured, this counter electrode permitted electrodeposition across the entire area of the carbon paper. The peroxymolybdic tungstate was reduced through bulk electrolysis, creating a blue film on carbon paper with a potential of -2.0 V for 20 – 120 minutes. Ultimately, these films were characterized by XPS (X-ray photoelectron spectroscopy).

Figure 4. A photo of electrodeposition experiment

Characterization of Films

To evaluate the nature of the prepared films, samples have been sent for determining conductivity, thickness, and X-ray photoelectron spectroscopy. Samples have been mailed to Oklahoma State University for conductivity and film thickness by Dr. Toby Nelson using the

Bruker DektakXT® Stylus Profiler (which utilized a cantilever deflection) and 4-point probe with a Keithley 2400 source meter (Results are pending due to lab closure). Samples were also sent to Dr. Nicholas Materer at Oklahoma State University for XPS to confirm the presence of molybdenum and tungsten. The XPS system uses a Physical Electronics (PHI Industries Inc.) dual pass cylinder-shaped mirror analyzer with a 50eV accompanied by PHI Mg anode with 300 W dual anode X-ray resource.

CO_2 Electrochemical Reduction

The experimental setup for electrochemical reduction of CO_2 is shown below in Figure 5.

Figure 5. The employed electrochemical cell for the reduction trial of CO_2 in the lab

The cathode compartment included both the Ag/AgCl reference electrode and the hydrogen molybdenum tungsten bronze film as a working electrode. The area of the film in solution for each trial was approximately 1.3 cm^2. The anode comprised the platinized titanium counter electrode and 18.5 mL of DI water saturated with CO_2 and 2 mL of 0.8 M $NaHCO_3$. This solution was prepared by saturating 18.5 mL of 18.2 MΩ pure water with CO_2 utilizing a SodaStream® and adding 2 mL of 0.8 M $NaHCO_3$ with one drop of conc. H_2SO_4, adjusting the pH to 6. The salt bridge connected the anode and the cathode compartments. Carbon dioxide gas was bubbled into the cathode solution for an hour by using a CO_2 tank. Bulk electrolysis was applied using different potentials (-0.2, -0.4, -0.6, -0.8, -1.0, -1.2, and -1.4 V) for an hour in

which both time and entire charge (in Coulombs) was determined using CHI software which plotted current and potential.

Evaluating Products Through Ion Chromatography

Formate was the expected product. However, ion chromatography identified oxalate as the only main product, which was carried out using a Metrohm 930 IC in which a Metro Sep column a Supp 16-250/4.0 was utilized at 45°C and a 0.7 mL/min flow rate of Na_2CO_3 (3.6 mmol) employed as an eluent and 5 mmol H_2SO_4 was used as a chemical suppressor.[62] Dilution with 0.8 M $NaHCO_3$ was utilized for preparing formate standards. Formate, the original suspected product, has a retention time of 4.6 minutes, while oxalate appears at 21 to 26 minutes. The range in retention time is due to overuse, the column's failure, and is planned to be replaced. Calibration using a newer column is needed to quantify the amount of oxalate generated. The background chromatogram was obtained by bubbling CO_2 into the electrolyte for an hour at each applied potential.

Figure 6. Metrohm 930 ion chromatography

CHAPTER 3. RESULTS AND DISCUSSION

Characterization of Electrodeposited Films

As mentioned previously, bulk electrolysis was carried out by utilizing the yellow solution of peroxymolybdic tungstate acid for the electrodeposition of the molybdenum tungsten hydrogen bronze films at an applied potential of -2.0 V. These films are blue when H^+ ion intercalated to a solid matrix. Figures 7 and 8 show the C-paper before and after electrodeposition.

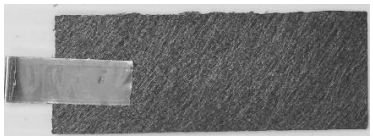

Figure 7. C-paper before the electrodeposition

Figure 8. The film of hydrogen bronze after 7200 seconds of electrodeposition on the C-paper

Film's XPS Characterization

The XPS of carbon paper and carbon paper with the electrodeposited hydrogen bronze film is shown in Figure 9. The blue line represents hydrogen bronze film while the orange line represents the carbon paper only. This spectrum proves that molybdenum (230 eV) and tungsten (425 eV) are in the electrodeposited film. Due to the carbon paper and hydrogen bronze film being exposed to air, oxygen (531 eV) is observed in both samples. However, the peak for oxygen is more intense for the electrodeposited film and the film is blue in color, which is similar to prepared hydrogen bronzes.[33]

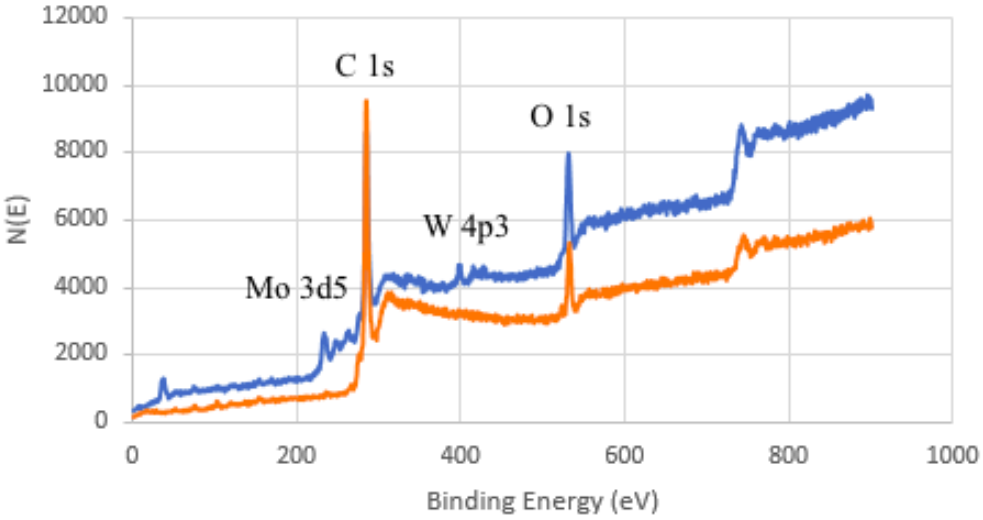

Figure 9. The combination of electrodeposited MoW bronze film's XPS spectrum and XPS spectrum for carbon paper only

Cyclic Voltammetry of the CO_2 Reduction

The CV of the C-paper only in CO_2 saturated with 0.8 M $NaHCO_3$ was carried out and shown in Figure 10. The same experiment using a molybdenum tungsten hydrogen bronze film on carbon paper is shown in Figure 11.

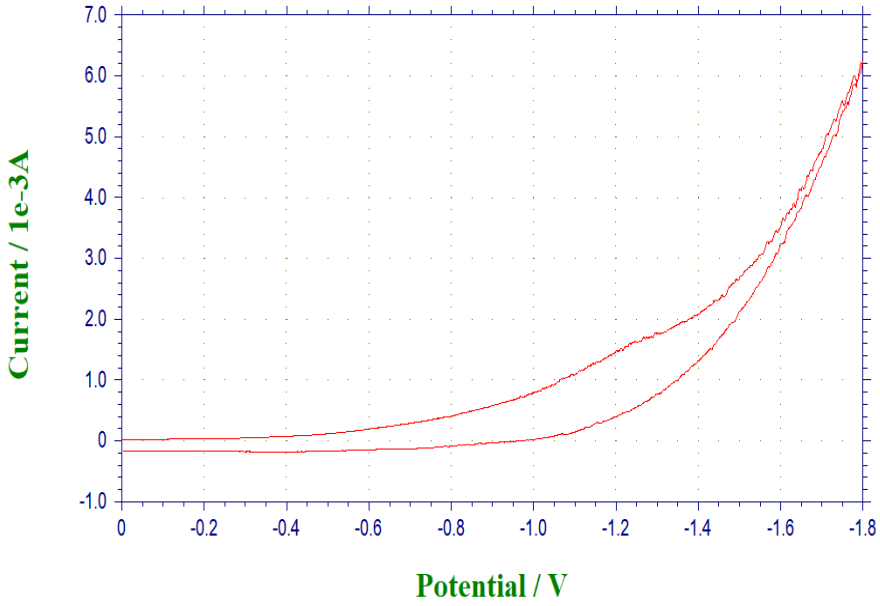

Figure 10. The CV of carbon paper in CO_2 saturated with $NaHCO_3$ (0.8 M) using the silver chloride as a reference electrode

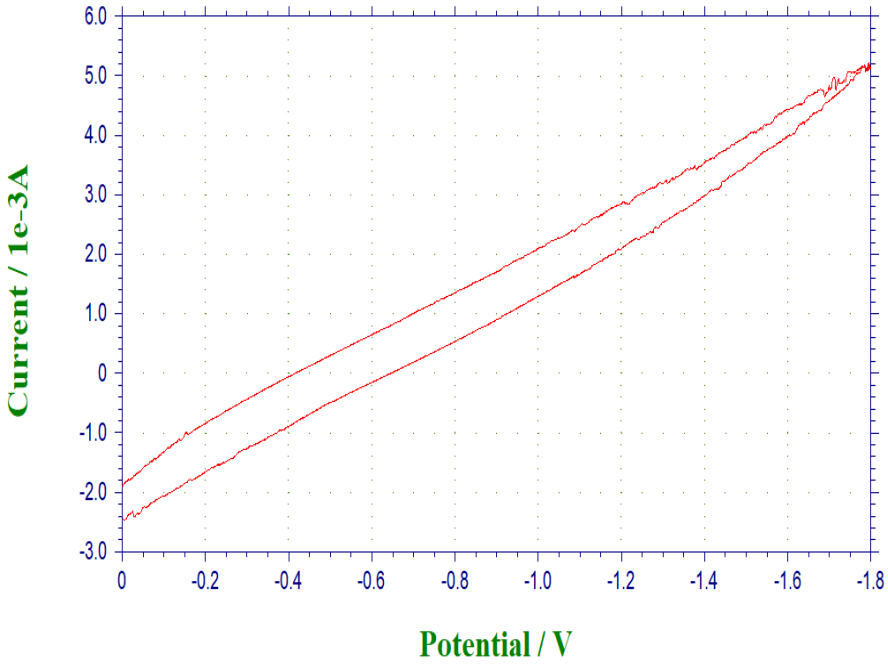

Figure 11. The CV of carbon paper with the molybdenum tungsten hydrogen bronze film and CO_2 gases saturated with $NaHCO_3$ (0.8 M) employing the reference electrode, which is Ag/AgCl

Comparing Figures 10 and 11, the current is larger and started at an applied potential of -0.6 V using the hydrogen molybdenum tungsten bronze film compared to carbon paper only that may indicate the film's enhanced electrochemical behavior toward electrochemical CO_2 reduction. Although, the current is slightly higher with hydrogen molybdenum tungsten bronze film at an applied potential of - 0.6 V, Figure 11 does not definitively show that the hydrogen bronze film is electrocatalytic toward CO_2 reduction. In order fully understand the cyclic voltammetry studies for CO_2 reduction, further experimentation is needed. This involves a control experiment (CVs in the absence of CO_2) to verify Figure 11. However, the control experiment has not been completed due to lab closure.

Evaluation for CO_2 Reduction Products

Formate was expected to be the product and the 930 IC was calibrated for detecting formate. Figure 12 shows a typical ion chromatogram identifying formate in 0.8 M $NaHCO_3$.

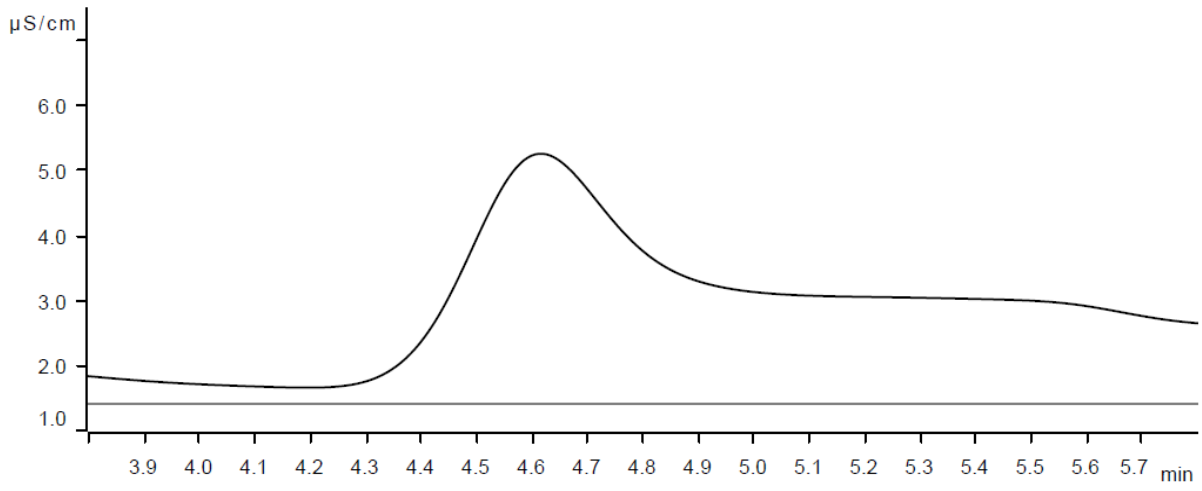

Figure 12. Typical ion chromatogram of conductivity (µS/cm) and time (minutes) identifying formate in 0.8 M $NaHCO_3$ with a retention time of 4.6 minute

For preparing the standard solutions, a 1,000-ppm standard of formate solution was diluted using $NaHCO_3$ (0.8 M) to prepare standard solutions. Figure 13 is a plot of peak area and formate concentration.

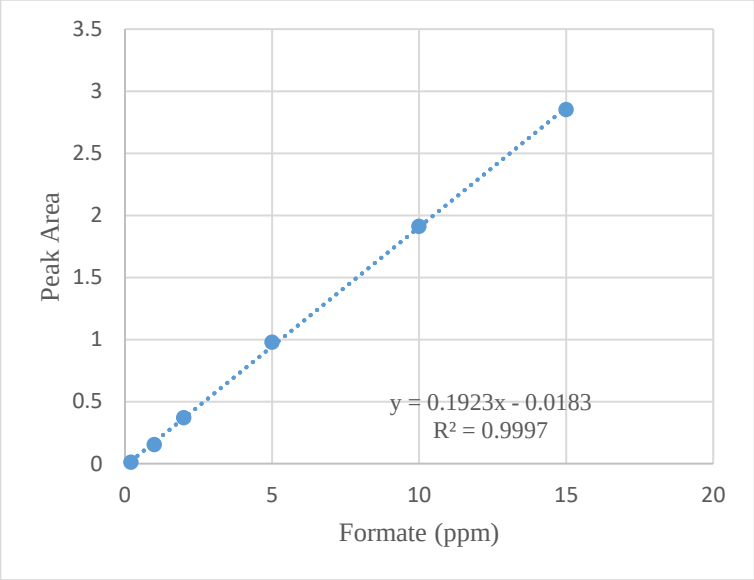

Figure 13. Calibration of the IC for projected yield formate

For evaluating the Faradaic efficiency, Equation (11) may be used for determining FE for the CO_2 reduction to formate.[63]

$$\varepsilon = \frac{n_{formate} nF}{Q} X\ 100\%. \qquad (11)$$

Where F = 96,485 Coulombs/mol (Faraday's constant), ε is FE, $n_{formate}$ is the formate's mole, Q is the charge for the CO_2 reduction period, and n is the e^- for the reduction of CO_2 gas to formate. However, ion chromatography following electrochemical reduction of CO_2 using the prepared films did not identify formate as a major reduction product. Figure 14 shows the ion chromatogram of the electrolyte using carbon paper only and an electrodeposited film at an applied potential of -0.6 V.

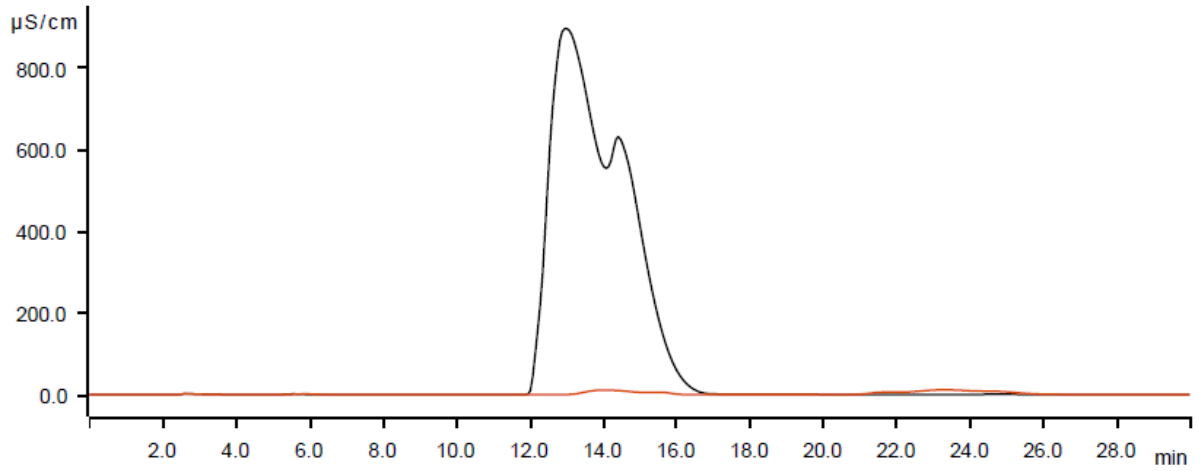

Figure 14. Ion chromatogram of electrolyte using carbon paper only and the deposited molybdenum tungsten bronze film at an applied potential of -0.6 V. (Red line represents molybdenum tungsten bronze film while black line represents carbon paper only)

Sulfuric acid appears with a retention time between 12 and 16 minutes, which is not surprising as sulfuric acid was used to adjust the electrolyte's pH to 6.0 before carrying out reduction experiments. The hydrogen bronze film in Figure 14 exhibited the sulfate peak could be less compared to the carbon paper only due to the possible reduction of sulfate. The main reduction product, thiosulfate, may have a similar retention time as oxalate at retention time between 21 to 26 minutes as shown in Figure 15. Some additional experiments need to be done in order to verify the presence of oxalate or other sulfate reduction compounds. Formate was an expected product. However, there is no peak with a retention time consistent with formate. Another unexpected very broad peak is observed at a retention time between 21 to 26 minutes. An expanded view of the chromatogram is shown in Figure 15.

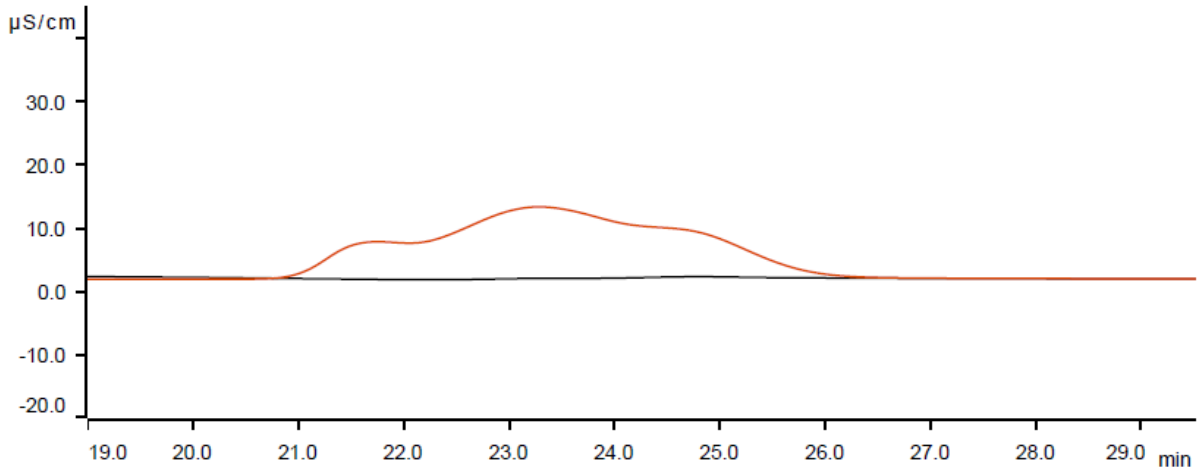

Figure 15. Ion chromatogram from 19 to 29 minutes of electrolyte using carbon paper only and the deposited molybdenum tungsten bronze film at an applied potential of -0.6 V. (Red line represents molybdenum tungsten bronze film while black line represents carbon paper only)

The peak in Figure 15 is possibly oxalate, which is a known reduction product in CO_2 reduction. Analyzing oxalic acid has the same retention time range. Just like in Figure 3, the mixed molybdenum tungsten hydrogen bronze film may act as a bimetal center fixing CO_2 and carry out an electrochemical reduction to oxalate. After reduction, the electrolyte at a pH of 6 extracts the oxalate anion. If this is indeed the case, then this is the first report of using a bimetal hydrogen bronze film for reduction of CO_2 selectively to two products based on ion chromatography. Ion chromatograms using other potentials are provided in Appendix 1. The most useful potential for conversion CO_2 to oxalate was at -0.6 V vs. the silver chloride reference, which is reasonably close to the standard reduction potential of -0.590 V vs. SHE. The standard reduction potential of CO_2 to oxalate is approximately -0.5 V meaning the overpotential is 0.1 V.[64] However, retention time alone is not definitive for oxalate.

According to the 10th edition of Quantitative Chemical Analysis by Harris and Lucy, sulfate can be reduced to thiosulfate near -0.6 V, which would have a longer retention time than sulfate and possibly overlap with oxalate. An experiment currently being planned and underway

is converting of oxalate to an insoluble magnesium crystal salt for single crystal X-ray diffraction carried out by Dr. Cassandra Eagle. Identifying magnesium oxalate from the electrolyte will definitively prove that oxalate is a reduction product using the hydrogen molybdenum tungsten bronze film. Additionally, a new ion chromatography column is in the process of being obtained and this experiment will be repeated to verify the presence of oxalate and/or thiosulfate as reduction products. Headspace experiments are also planned to look for gaseous products such as CO and possibly hydrocarbons. Table 2 summarizes the peak areas for the amount of suspected oxalate product using hydrogen molybdenum tungsten bronze films and carbon paper only. These values have not been converted to moles or concentrations due to the required closure of the lab and the column's failure, which did not permit calibrating the ion chromatogram. Repeating these trials at -0.6 V and confirmatory experiments are planned.

Table 2. Applied potential and peak areas for suspected oxalate using hydrogen molybdenum tungsten bronze films and carbon paper

Potential	Oxalate peak area (bronze film)	Oxalate peak area (Carbon paper only)
(V)	(μS·cm)	(μS·cm)
-1.4	0.059	0.009
-1.2	0.021	0.003
-1	0.113	0.006
-0.8	0.015	0.008
-0.6	0.129	0.008
-0.4	0.098	0.003
-0.2	0	0

These experiments show that reduction of CO_2 to oxalate may be possible. The maximum amount of oxalate was obtained at an applied potential of – 0.6 V. This work shows that electrodeposited molybdenum and tungsten bronze films are useful in reduction of CO_2.

CHAPTER 4. CONCLUSIONS

The goal of this project was to prepare mixed hydrogen molybdenum tungstate bronze films using electrodeposition and carry out the electrochemical reduction of CO_2. The combination of sodium molybdate and sodium tungstate when dissolved in saturated water with hydrogen peroxide and sulfuric acid resulted in a yellow peroxy-metal solution. Bulk electrolysis generated a blue film deposited on carbon paper. The carbon paper for depositing the hydrogen molybdenum tungstate bronze films was used to electrochemically reduce CO_2 at different potentials vs. the Ag/AgCl reference electrode. Reduction of CO_2 at various potentials was carried out using film-modified carbon paper and products were evaluated by ion chromatography.[33] These films are easy to prepare and cheap. X-ray photoelectron spectroscopy confirmed the presence of molybdenum, tungsten, and oxygen, indicating the film is most likely a hydrogen bronze. Cyclic voltammetry was carried out using both carbon paper only and carbon paper with hydrogen bronze films in carbon saturated with 0.8 M $NaHCO_3$ as electrolyte. Compared to carbon paper only, when using the hydrogen molybdenum tungsten bronze film as the working electrode, oxalate was the most likely product obtained using an applied potential of –0.6 V vs. the silver chloride reference electrode. Further work is needed to identify these products definitively. Future work includes using other bronzes such as vanadium as the oxide form is a known catalyst for oxalate synthesis to improve the overall yield. Also, electrodeposition for longer times and lower current to determine the effect on the crystalline structure.

REFERENCES

1. Najafabadi, A. (2013). CO_2 chemical conversion to useful products: An engineering insight to the latest advances toward sustainability. *International Journal of Energy Research*, 37: 485-499.
2. Abraham, J. Scientists Study Ocean Absorption of Human Carbon Pollution. *The Guardian*. Retrieved from: https://www.theguardian.com/environment/climate-consensus-97-per-cent/2017/feb/16/scientists-study-ocean-absorption-of-human-carbon-pollution.
3. Ganesh, I. (2014). Conversion of carbon dioxide into methanol– a potential liquid fuel: Fundamental challenges and opportunities (a review). *Renewable and Sustainable Energy Reviews*, 31: 221-257.
4. Statista. (2020). Projected CO_2 Emissions Worldwide 2050. *Statista*. Retrieved from https://www.statista.com/statistics/263980/forecast-of-global-carbon-dioxide-emissions.
5. Stein, T. Another Climate Milestone on Mauna Loa. *National Oceanic and Atmospheric Administration*. Retrieved from: https://research.noaa.gov/article/ArtMID/587/ArticleID/2362/Another-climate-milestone-falls-at-NOAA%E2%80%99s-Mauna-Loa-observatory. (accessed November 2,2020).
6. Wu, J. & Zhou, X. (2016). Catalytic conversion of CO_2 to value added fuels: Current status, challenges, and future directions. *Chin. J. Catal*., 37: 999–1015.
7. Miller, H. et al. (2018). Improving the Energy Efficiency of Direct Formate Fuel Cells with a Pd/C-CeO_2 Anode Catalyst and Anion Exchange Ionomer in the Catalyst Layer. *Energies*, 11(2):369-381. (accessed October 19,2020).
8. Ren, M. et al. (2011). Regenerative Methanol Fuel Cells: Reduction of CO_2 to Methanol on Oxidized Cu Electrodes. *The Electrochemical Society Transitions*, 33(39): 253-259.

9. An, L. & Chen, R. (2016). Direct Formate Fuel Cells: A Review. *J. Power Sources*, 320: 127–139.
10. Kaneco, S., et al. (2006). Electrochemical Reduction of CO2 to Methane at the Cu Electrode in Methanol with Sodium Supporting Salts and its Comparison with Other Alkaline Salts. *Energy Fuels*, 20(1): 409-414.
11. Albo, J. et al. (2012). Toward the electrochemical conversion of carbon dioxide into methanol. *The Royal Society of Chemistry.* DOI: 10.1039/x0xx00000x. https://pubs.rsc.org/en/content/articlelanding/2015/gc/c4gc02453b#!divRelatedContent (accessed October 20,2020).
12. Sun, Z. et al. (2017). Fundamentals and Challenges of Electrochemical CO_2 Reduction Using Two-Dimensional Materials. *Chem., Cell Press*, 3: 560–587.
13. Olah, G., Goeppert, A. & Prakash, G. (2008). Chemical Recycling of Carbon Dioxide to Methanol and Dimethyl Ether: From Greenhouse Gas to Renewable, Environmentally Carbon Neutral Fuels and Synthetic Hydrocarbons. *The Journal of Organic Chemistry*, 74: 487-498.
14. Pokharel, UR., Fronczek, FR. & Maverick, AW. (2014). Reduction of carbon dioxide to oxalate by a binuclear copper complex. *Nature Communications*, 5(5883), 1-5. https://www.nature.com/articles/ncomms6883. (accessed December 11,2020).
15. Subramanian, S. et al. (2020). New insights into the electrochemical conversion of CO_2 to oxalate at stainless steel 304L cathode. *Journal of CO_2 Utilization*, 36: 105-115.
16. Qiao, J., Liu, Y. & Zhang, J. (2014). A Review of Catalysts for the Electroreduction of Carbon Dioxide to Produce Low-Carbon Fuels. *Chem. Soc. Rev.*, 43(2): 631–675.

17. Pocaznoi, D., Calmet, A., Etcheverry, L., Erable, B. and Bergel, A., (2012). Stainless steel is a promising electrode material for anodes of microbial fuel cells. *Energy & Environmental Science*, *5*(11): 9645-9652.

18. Lv, W.X., Zhang, R., Gao, P.R., Gong, C.X. and Lei, L.X., (2013). Electrochemical reduction of carbon dioxide on stainless steel electrode in acetonitrile. In *Advanced Materials Research*, 807:1322-1325.

19. Hori, Y., Kikuchi, K. & Suzuki, S. (1985). Production of CO and CH_4 in Electrochemical Reduction of CO_2 at Metal Electrodes in Aqueous Hydrogencarbonate Solutions. *Chem. Lett*, 14: 1695-1698.

20. Nitopi, S. et al. (2019). Progress and Perspectives of Electrochemical CO_2 Reduction on Copper in Aqueous Electrolyte. *Chem. Rev.*, 119(12): 7610–7672.

21. Hori, Y. (2008). Electrochemical CO_2 Reduction on Metal Electrodes. In: Vayenas C.G., White R.E., Gamboa-Aldeco M.E. (eds). *Modern Aspects of electrochemistry*, vol 42. Springer, New York, NY. https://doi.org/10.1007/978-0-387-49489-0_3.

22. Pérez-Rodríguez, S. et al. (2011). Carbon-Supported Fe Catalysts for CO_2 Electroreduction to High-Added Value Products: A DEMS Study: Effect of the Functionalization of the Support. *International Journal of Electrochemistry*, 2011(249804): 1-13.

23. Choi, SY. et al. (2016). Electrochemical Reduction of Carbon Dioxide to Formate on Tin–Lead Alloys. *ACS sustainable. Chem. Eng*., 4: 1311-1318.

24. Kortlever, R. et al. (2015). Electrochemical CO_2 Reduction to Formic Acid at Low Overpotential and with High Faradaic Efficiency on Carbon-Supported Bimetallic Pd–Pt Nanoparticles. *ACS Catal*. pp 3916-3923.

25. Min, X. & Kanan, MW. (2015). Pd-Catalyzed Electrohydrogenation of Carbon Dioxide to Formate: High Mass Activity at Low Overpotential and Identification of the Deactivation Pathway. *J. Am. Chem. Soc*. 137(14): 4701-4708.

26. Hu, X. (2018). Selective CO_2 Reduction to CO in Water using Earth-Abundant Metal and Nitrogen-Doped Carbon Electrocatalysts. *ACS Catal*. pp. 6255-6264.

27. Spinner, N., Vega, J. & Mustain, W. (2012). Recent progress in the electrochemical conversion and utilization of CO_2. *Catalysis Science & Technology*, 2: 19-28.

28. Bonetto, R., Crisanti, F. & Sartorel, A. (2020). Carbon Dioxide Reduction Mediated by Iron Catalysts: Mechanism and Intermediates That Guide Selectivity. *ACS Omega*, 5: 21309-21319.

29. Chung, DW. et al. (2014). Inhibition of CO poisoning on Pt catalyst coupled with the reduction of toxic hexavalent chromium in a dual-functional fuel cell. *Scientific Reports*, 4: 7450-7454.

30. Chen, L. et al. (2008). On the Mechanisms of Hydrogen Spillover in MoO_3. *J. Phys. Chem. C*., 112: 1755-1758.

31. Hu, XK. et al. (2008). Comparative Study on MoO_3 and $HxMoO_3$ Nanobelts: Structure and Electric Transport. *Chem. Mater*., 20(4): 1527-1533.

32. Sha, X. (2009). Hydrogen Absorption and Diffusion in Bulk α-MoO3. *J. Phys. Chem. C*., 113: 11399-11407.

33. Cui, Y. et al. (2019). Discoloration Effect and One-Step Synthesis of Hydrogen Tungsten and Molybdenum Bronze ($HxMO_3$) using Liquid Metal at Room Temperature. *ACS Omega*, 4: 7428-7435.

34. Gui, Y. & Blackwood, DJ. (2014). Electrochromic Enhancement of WO_3-TiO_2 Composite Films Produced by Electrochemical Anodization. *J. Electrochem. Soc*., 161: E191-E201.

35. Pathan, H. et al. (2006). Electrosynthesis of molybdenum oxide thin films onto stainless substrates. *E-chem comms.* pp. 273-278.

36. Summers, D. P.; Steven, L.; Karl W. F. (1986). The electrochemical reduction of aqueous carbon dioxide to methanol at molybdenum electrodes with low overpotentials, *J. Electroanalytical Chem. Interfacial Elec*. pp. 219-232.

37. Ayyappan, S.; Rao, C. N. R. (1995). A Simple Method of Hydrogen Insertion in Transition Metal Oxides to Obtain Bronzes. *Mater. Res. Bull*. pp. 947-951.

38. Ressler, T.; Wienold, J.; Jentoft, R. E. (2001). Formation of Bronzes during Temperature programmed Reduction of MoO_3 with Hydrogen- an in situ XRD and XAFS Study. *Solid State Ionics*. pp. 141-142, 243-251.

39. Materer, N. et al. (2016). The preparation and chemical reaction kinetics of tungsten bronze thin films and nitrobenzene and without a catalyst. *Surface Science,* 648: 345-351.

40. Li, YF. (2020). Hydrogen Bronzes of WO_3 and MoO_3 as Active (Photo-) Catalyst Supports for CO_2 Reduction. PhD Thesis; *University of Toronto*. Retrieved from https://tspace.library.utoronto.ca/bitstream/1807/101211/4/Li_Young_Feng_202006_PhD_thesis.pdf.

41. Cong, S., Geng, F. & Zhao, Z. (2016). Tungsten Oxide Materials for Optoelectronic Applications. *Advanced Materials*, 28(47): 10518–10528.

42. Huang, ZF. et al. (2015). Tungsten Oxides for Photocatalysis, Electrochemistry, and Phototherapy. *Advanced Materials*, 27(16): 5309-5327.

43. Zhu, T., Chong, MN. & Chan, ES. (2014). Nanostructured Tungsten Trioxide Thin Films Synthesized for Photoelectrocatalytic Water Oxidation: A Review. *ChemSusChem*., 7(11): 2974–2997.

44. Song, J. et al. (2015). Oxygen-Deficient Tungsten Oxide as Versatile and Efficient Hydrogenation Catalyst. *ACS Catal*, 5(11): 6594–6599.

45. Wang, L. et al. (2016). Hydrogen-Treated Mesoporous WO_3 as a Reducing Agent of CO_2 to Fuels (CH_4 and CH_3OH) with Enhanced Photothermal Catalytic Performance. *J. Mater. Chem. A.*, 4(14): 5314–5322.

46. Zhang, N. et al. (2016). Oxide Defect Engineering Enables to Couple Solar Energy into Oxygen Activation. *J. Am. Chem. Soc*., 138(28): 8928–8935.

47. Kondrachova, L. et al. (2006). Cathodic Electrodeposition of Mixed Molybdenum Tungsten Oxides from Peroxo-polymolybdotungstate Solutions. *Langmuir*, 22(25), 10490-10498.

48. Li, XP. Et al. (2013). Hydrogen Tungsten Bronze-Supported Platinum as Electrocatalyst for Methanol Oxidation. *Fuel Cells*, 13: 314–318.

49. Taube, F. et al. (2002). Characterization of aqueous peroxomolybdate catalysts applicable to pulp bleaching. *J. Chem. Soc., Dalton Trans.***,** 2002(6): 1002–1008.

50. Ozensoy, E. (1979). Separation of Molybdenum from Tungsten Solutions by Solvent Extraction Using Hydrogen Peroxide. PhD Thesis; *University of London.* Department of Metallurgy and Materials Science. Royal School of Mine.

51. Van, C. et al. (1991). Preparation of High Surface Area Hydrogen Molybdenum Bronze Catalysts. *Studies in Surface Science and Catalysis*, 63: 679-686.

52. Scott, DW. & Alharbi, S. (2020). Electrodeposition of Hydrogen Molybdenum Bronze Films and Electrochemical Reduction of Carbon Dioxide. *Journal of Thin Films Research*, 4(1), 46-50.

53. Gawande, M., Pandey, R. & Jayaram, R. (2012). Role of mixed metal oxides in catalysis science-versatile applications in organic synthesis. *Catal. Sci. Technol.*, 2(6): 1113-1125.

54. Amrute, AP. et al. (2008). Sol–Gel Synthesis of MoO_3/SiO_2 Composite for Catalytic Application in Condensation of Anisole with Paraformaldehyde. *Catal. Lett*., 126(286): 286-292.

55. Biradar, AV., Umbarkar, SV. & Dongare, MK. (2005). Transesterification of diethyl oxalate with phenol using MoO_3/SiO_2 catalyst. *Applied Catalysis A General*, 285(1): 190-195.

56. Gawande, MB. & Jayaram, RV. (2006). A novel catalyst for the Knoevenagel condensation of aldehydes with malononitrile and ethyl cyanoacetate under solvent free conditions. *Catalysis Communications*, 7(12): 931–935.

57. Singh, SJ. & Jayaram, RV. (2008). Chemoselective O-tert-butoxycarbonylation of hydroxy compounds using $NaLaTiO_4$ as a heterogeneous and reusable catalyst. *Tetrahedron Letters*, 49(27): 4249-4251.

58. Ikeda, S., Ito, K. & Noda, H. (2009). Electrochemical Reduction of Carbon Dioxide Using Gas Diffusion Electrodes Loaded with Fine Catalysts. *AIP Conference Proceedings*, 1136(1): 108-113.

59. Baoxing, W. & Shaojun, D. (1994). Electrocatalytic properties of mixed-valence molybdenum oxide thin film modified microelectrodes. *Journal of Electroanalytical Chemistry*, 379: 207-214.

60. Yamanaka, K. (1987). Electrodeposited Films from Aqueous Tungstic Acid-Hydrogen Peroxide Solutions for Electrochromic Display Devices. *Japanese Journal of Applied Physics,* 26(11): 1884-1890.

61. Koçak, S., Ertaş, F. & Dursun, Z. (2013). Electrochemical deposition and behavior of mixed-valent molybdenum oxide film at glassy carbon and ITO electrodes. *Applied Surface Science,* 265: 205-213.

62. Borgschulte, A. et al. (2017). Hydrogen Reduction of Molybdenum Oxide at Room Temperature. *Sci. Reports,* 7(40761): 1-12.

63. Weixin, L. et al. (2014). Studies on the Faradaic Efficiency for Electrochemical Reduction of Carbon Dioxide to Formate on Tin Electrode. *J. Power Sources,* 253: 276-281.

64. Yang, N., Waldvogel, S. & Jiang, X. (2015). Electrochemistry of Carbon Dioxide on Carbon Electrode. *ACS Appl. Mater. Interfaces*, 8: 28357−28371.

APPENDIX: Ion Chromatograms Using Other Potentials

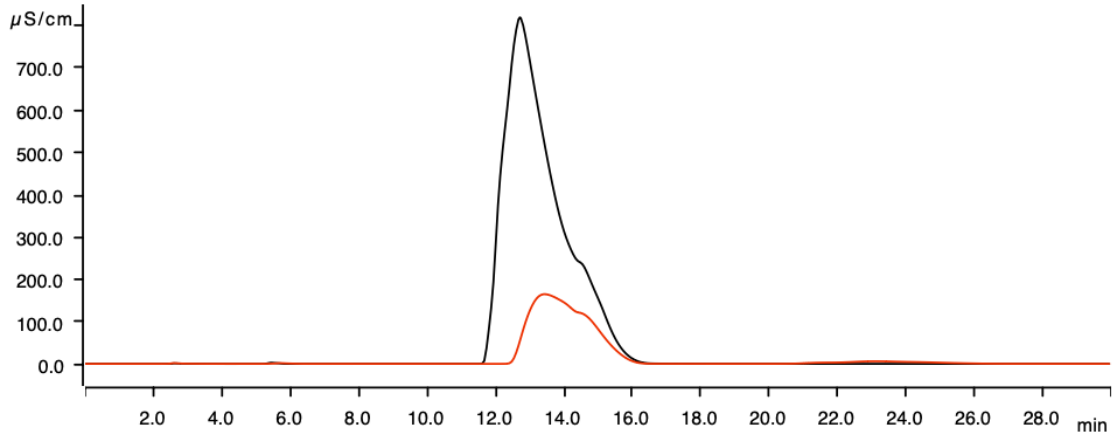

Figure 16 (A1). Ion chromatogram of electrolyte using carbon paper only and the deposited molybdenum tungsten bronze film at an applied potential of -0.4 V

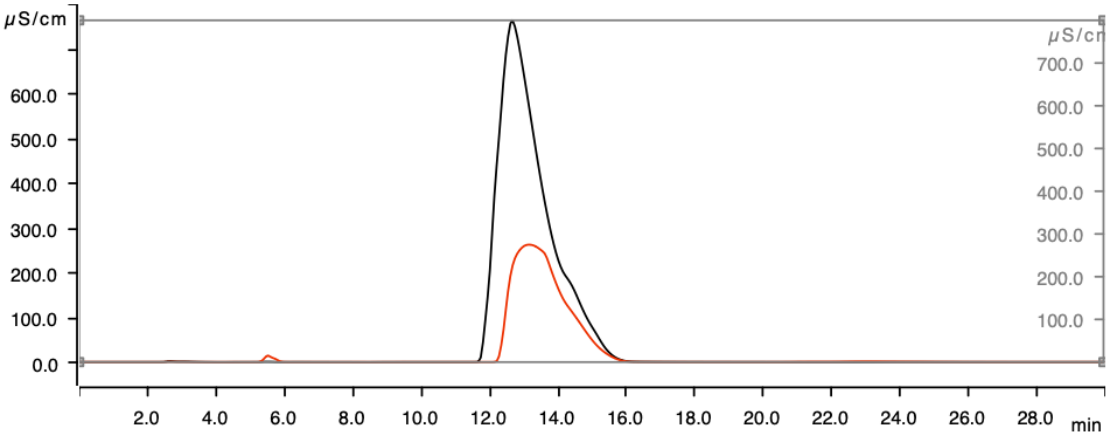

Figure 17 (A2). Ion chromatogram of electrolyte using carbon paper only and the deposited molybdenum tungsten bronze film at an applied potential of -0.8 V

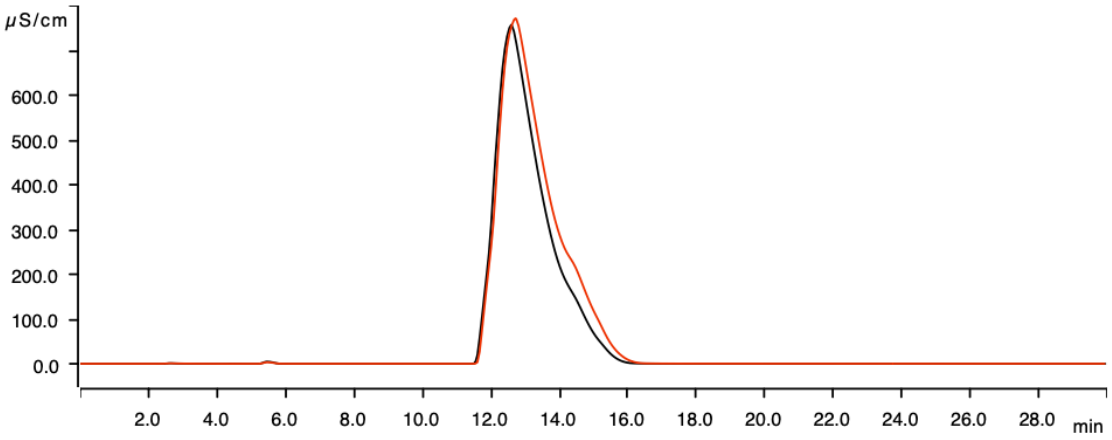

Figure 18 (A3). Ion chromatogram of electrolyte using carbon paper only and the deposited molybdenum tungsten bronze film at an applied potential of -1.0 V

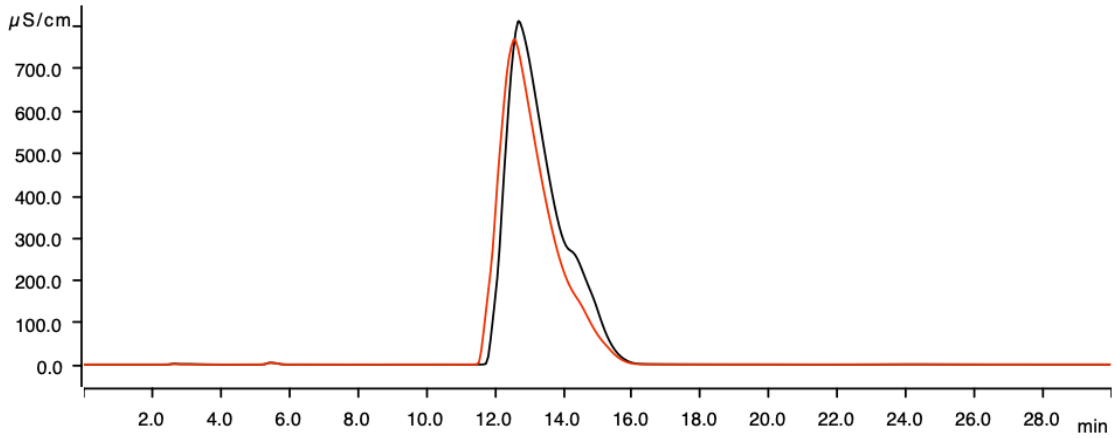

Figure 19 (A4). Ion chromatogram of electrolyte using carbon paper only and the deposited molybdenum tungsten bronze film at an applied potential of -1.2 V

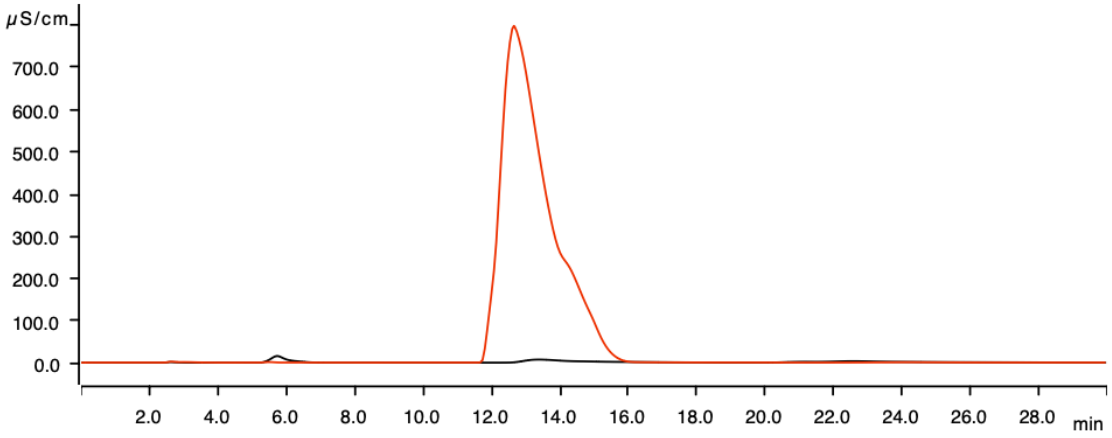

Figure 20 (A5). Ion chromatogram of electrolyte using carbon paper only and the deposited molybdenum tungsten bronze film at an applied potential of -1.4 V

VITA

MOHAMMAD SAEED BAJUNAID

Education:	M.A. Chemistry, East Tennessee State University, Johnson City, Tennessee, (May 2021)
	B.A. Chemistry, King Abdulaziz University, Jeddah, Saudi Arabia, (August 2015)
Professional Experience:	Teaching Assistant, King Saud bin Abdulaziz University for Health and Sciences; Riyadh, Saudi Arabia, (September 2016- June 2017)
Presentation and Award:	Mohammad Bajunaid, *Dane W. Scott. Electrodeposition of Hydrogen Molybdenum Tungsten Bronze Films and Electrochemical Reduction of Carbon Dioxide
	SERMACS 2019 chemistry on the coast, Savannah, GA, (10/23/2019), poster presentation
	Eastman-NETSACS Student Research Symposium, Kingsport, TN, (10/9/2019), poster presentation, scholarship award for SERMACS 2019 conference